AAEC/E646

AUSTRALIAN ATOMIC ENERGY COMMISSION

RESEARCH ESTABLISHMENT

LUCAS HEIGHTS RESEARCH LABORATORIES

THEORETICAL MODELS TO PREDICT THE TRANSIENT HEAT TRANSFER PERFORMANCE OF HIFAR FUEL ELEMENTS UNDER NON-FORCED CONVECTIVE CONDITIONS

by

W. J. GREEN

APRIL 1987

ISBN 0 642 59859 2

AUSTRALIAN ATOMIC ENERGY COMMISSION
RESEARCH ESTABLISHMENT

LUCAS HEIGHTS RESEARCH LABORATORIES

THEORETICAL MODELS TO PREDICT THE TRANSIENT HEAT TRANSFER PERFORMANCE OF HIFAR FUEL ELEMENTS UNDER NON-FORCED CONVECTIVE CONDITIONS

by

W.J. GREEN

ABSTRACT

Simple theoretical models have been developed which are suitable for predicting the thermal responses of irradiated research reactor fuel elements of markedly different geometries when they are subjected to loss-of-coolant accident conditions. These models have been used to calculate temperature responses corresponding to various non-forced convective conditions, and comparisons have been made between experimentally observed temperatures and calculated values. These comparisons have shown that

(a) a suitable value for surface thermal emissivity is 0.35;

(b) modelling of the fuel element beyond the region of the fuel plate needs to be included since these areas account for approximately 25 per cent of the thermal power dissipated - however, detailed modelling of these end regions was not found to be critical;

(c) general agreement between calculated and experimental temperatures for both transient and steady-state conditions is good - the maximum discrepancy between calculated and experimental temperatures for a HIFAR Mark IV/V fuel element is ~70°C, and for an Oak Ridge Reactor (ORR) box-type fuel element ~30°C; and

(d) axial power distribution does not significantly affect thermal responses for the conditions investigated.

Overall, the comparisons have shown that the models evolved can reproduce experimental data to a level of accuracy that provides confidence in the modelling technique and the postulated heat dissipation mechanisms, and that these models can be used to predict thermal responses of fuel elements in accident conditions that are not easily investigated experimentally.

National Library of Australia card number and ISBN 0 642 59859 2

The following descriptors have been selected from the INIS Thesaurus to describe the subject content of this report for information retrieval purposes. For further details please refer to IAEA-INIS-12 (INIS: Manual for Indexing) and IAEA-INIS-13 (INIS: Thesaurus) published in Vienna by the International Atomic Energy Agency.

EMISSIVITY; EXPERIMENTAL DATA; FUEL ELEMENTS; H CODES; HEAT TRANSFER; HIFAR REACTOR; LOSS OF COOLANT; MATHEMATICAL MODELS; NATURAL CONVECTION; ORR REACTOR; RADIANT HEAT TRANSFER; SPECIFIC HEAT; THERMAL CONDUCTION; THERMAL CONDUCTIVITY; THERMAL DIFFUSIVITY; THEORETICAL DATA

EDITORIAL NOTE

From 27 April 1987, the Australian Atomic Energy Commission (AAEC) is replaced by Australian Nuclear Science and Technology Organisation (ANSTO). Serial numbers for reports with an issue date after April 1987 have the prefix ANSTO with no change of the symbol (E, M, S or C) or numbering sequence.

CONTENTS

1. INTRODUCTION

Prediction of the thermal response of an irradiated fuel element which is subjected to a loss-of-coolant accident (LOCA) condition has received considerable attention during the last three decades. In the case of HIFAR and other DIDO class reactors, several LOCA conditions have been postulated which could occur when the fuel element

(i) is left in the reactor after reactor shutdown,

(ii) is being transported from the reactor to the storage facility, or

(iii) is contained in the storage pond.

In all cases, accident conditions are postulated in which either all the coolant water has escaped from the reactor (or storage pond), or the forced convective gas cooling used in transport devices has failed.

The parameters controlling the temperature responses in each type of problem are

(i) the fission product decay heat which is related to the time that has elapsed since the reactor was shut down,

(ii) the geometrical configuration of the fuel element, and

(iii) the external boundary conditions which dictate the mechanisms that dissipate heat from the fuel element.

Of the various possible LOCAs that have been postulated, the most credible was considered to be one which might occur during the unloading and transportation of irradiated fuel from the reactor to the storage facility. Normally, in such an unloading process, the irradiated fuel is lifted into a transport flask which has an internal fan-driven, air-cooling system that prevents the fuel from overheating. A safety problem arises, however, if this air-cooling system fails. Such a failure would cause the fuel element temperature to rise, and it is possible that temperatures could reach levels where the fuel cladding will blister and rupture, thereby releasing fission products hazardous to reactor personnel. Consequently, it is important for the reactor operator to know how long the fuel must remain in the shut-down water-cooled reactor in order to reduce decay heat to a level where fuel plate damage will not occur if the transport flask air-cooling system fails.

Direct information on this type of problem has been obtained for the HIFAR reactor by conducting special experiments which used an irradiated mark IV/V fuel element contained in the HIFAR load/unload flask without the cooling system in operation [Parsons 1971]. Such specific experimentation has provided pertinent operator guidelines for a particular assembly but is not suitable for predicting the thermal performance of different fuel element designs or under different external conditions.

Moreover, temperatures have also been recorded for irradiated ORR (Oak Ridge Reactor) fuel elements when they are cooled in stagnant air [Wett 1960]. These experiments involved box-type fuel elements which, after various periods of irradiation were withdrawn from the Oak Ridge Reactor, transported to a hot cell and then hung in free space so that they were cooled only by natural convection and thermal radiation.

Apart from practical experiments, calculations have been performed to estimate temperature responses of HIFAR IV/V fuel elements situated in stagnant air [Green 1973, 1974]. These calculational studies made several conservative assumptions and no attempt was made to relate theoretical models to experimental results. Over the years, there has been a continued interest [*e.g.* J. Connolly 1984, AAEC private communication] in developing calculational methods capable of ascertaining HIFAR fuel element temperature responses under LOCA conditions. The objective was to develop a calculational model which can be used to predict 'ever-safe' accident conditions.

Recently, the AAEC endorsed a proposal to develop theoretical heat transfer models to analyse and reproduce experimental results from HIFAR and from overseas reactors. It was stipulated that these models should be as simple as possible and be based on *common* hypotheses including rates of fission product decay heat generation and modes of heat transport. Such models, when developed, would enable prediction of thermal responses to be made for postulated accident conditions which cannot be easily simulated experimentally.

2. MATHEMATIC MODELLING OF PHYSICAL GEOMETRIES

In this work, theoretical models have been developed using the two-dimensional transient heat transfer code HEATRAN [Collier 1969]. This computer code is based upon finite elements and has been extensively used by the AAEC.

2.1 HIFAR Fuel Element

To model the HIFAR fuel element shown in **figure 1**, several criteria had to be considered. First, the model needed to represent, as realistically as possible, the most significant features of the actual fuel element. Second, there had to be enough calculational node points to give an adequate indication of thermal performance and yet not so many that either the code would not operate (there is a finite limitation on nodes), or computing times would be excessive.

Since HEATRAN is a two-dimensional code, an appropriate geometry had to be chosen (*i.e.* RZ or XY) for describing the fuel element. Although the HIFAR fuel element contains features such as the fuel positioning end combs which provide alternate conduction paths in the radial direction, in general, it is best represented by the RZ option, but non-circular geometrical features which may be significant also need to be considered. In the event, only the fuel plate end combs were important enough to merit special consideration in the RZ model. These combs were included in the RZ model by converting their volume into an imaginary thin annular disc extending from the inside diameter of the flux scan assembly (FSA) thimble to the external diameter of the outer sheath. Contact resistances between the fuel plates and the support combs were assumed to be negligible. The modelling of fuel element features above the level of the fuel plates was limited to

(i) extending the FSA thimble by 83.8 cm (corresponding to the actual height of the FSA), above the fuel plates, and

(ii) extending the outer sheath by 22.9 cm (corresponding to the approximate height of the outer sheath to where its diameter changes, see **figure 1**).

2.2 ORR Fuel Elements

Unlike the HIFAR fuel element, the ORR box-type fuel elements used in the experiments reported by Wett [1960] need a three-dimensional representation and do not readily reduce to a two-dimensional geometry. Several factors had to be examined in constructing suitable models. First, calculations performed for the HIFAR fuel element showed that the end effects were significant and would need to be taken into account when comparing calculated thermal responses and observed experimental data. Second, a cross-sectional view of the fuel element (see **figure 2**) is most readily modelled by XY co-ordinates which, however, excludes any modelling of axial and end effects.

Because of these two conflicting considerations, an XY model of a simplified quadrant of the cross-sectional plan of the fuel element was initially constructed (see **figure 3**) and used to determine temperature distributions within the fuel plates. This showed that temperature variations throughout the model were less than ±2% of the average absolute fuel plate temperature for the thermal power outputs to be investigated. It was thus concluded that the cross-sectional model could be converted to a cylindrical cross-section in which

(i) the external radius was fixed such that the external areas of the fuel element and the equivalent cylindrical model were the same;

(ii) calculation of the inside radius was based upon the cross-sectional areas of the equivalent cylindrical model and the real fuel element remains the same; and

(iii) the inside surface of the equivalent model was considered as a perfectly insulated boundary.

Converting the fuel element geometry to such an equivalent cylindrical configuration meant that the ORR fuel element could then be modelled in RZ co-ordinates with the inclusion of end extensions. However, to confirm that this RZ model accurately represented the thermal response of the XY model, comparative calculations were performed for the two models. The comparisons (see **figure 4**) showed that the cylindrical model with the end extensions eliminated gave essentially the same thermal response as the XY model.

3. SPECIFICATION OF INPUT DATA

3.1 HIFAR Fuel Elements

Appendix A lists typical data supplied to HEATRAN, with the nodal array and finite element structure listed under NODES and CONNECTIONS. For the particular data given in **appendix A**, the pictorial representation of the nodes and connections is shown in **figure 5**.

3.1.1 Material properties and heat sources

The material properties of the aluminium/fuel alloy and aluminium for the cladding, the FSA and external sheath, have been obtained from Lyman [1954], Eckert and Drake [1959], Weast [1971] and Houghtaling *et al.* [1964]. The data are summarised below:

Material	Density ($kg\ m^{-3}$)	Thermal Conductivity ($W\ cm^{-1}\ K^{-1}$)	Specific Heat ($kJ\ kg^{-1}\ K^{-1}$)
Al/fuel alloy	3172	1.3408	0.7995
Aluminium	2707	2.0414	0.8958

Preliminary investigations into the optimum design of the nodal model indicated that maximum calculational accuracy was achieved by specifying fuel plates with no internal nodes. Such a configuration meant that material properties for the overall fuel plate of aluminium cladding and aluminium/fuel alloy had to be determined. Composite properties were ascertained using the following formulae:

(i) Thermal conductivity

$$\kappa = \frac{\delta_c + \delta_f}{\frac{\delta_c}{\kappa_c} + \frac{\delta_f}{\kappa_f}} \quad ,$$

where δ_c is the total thickness of the Al cladding present in a fuel plate, κ_c is the thermal conductivity of the Al, δ_f is the thickness of the fuel alloy, and κ_f is the thermal conductivity of the fuel alloy.

(ii) Density

$$\rho = \frac{1}{(\delta_c+\delta_f)} \left\{ \rho_c\delta_c + \rho_f\delta_f \right\} \quad ,$$

where δ_c and δ_f are as above, ρ_c is the density of Al cladding, and ρ_f is the density of fuel alloy.

(iii) Specific heat

$$C_p = \frac{\rho_c c_{pc}\delta_c + \rho_f c_{pf}\delta_f}{(\delta_c+\delta_f)\rho} \quad .$$

When specifying the heat sources in the fuel plates it was assumed that

- the generation rate is independent of temperature,
- heat is generated over the full thickness of the fuel plate (*i.e.* including both the aluminium cladding and the central fuel alloy),
- heat is generated over a length of 603 mm, and
- the axial heat generation distribution is either uniform or of the idealised step function form which represents information given by Duerden [1972] - see **figure 6**.

As discussed later, conduction through gas is a significant heat transfer mechanism between fuel plates and hence needs to be specified with reasonable accuracy.

The relationship between gas conductivity and temperature, which was input to the model, is based upon data from Eckert and Drake [1959] for air at atmospheric pressure and is as follows:

$$\kappa_g = 0.000\,076\,64\,[1 + 0.003\,961\,6\,(Ti + Tj)],$$

where Ti and Tj are temperatures (K) of adjacent surfaces and κ_g is gas conductivity in W/cm °C.

3.1.2 Thermal boundary conditions

(a) Internal surfaces

For narrow vertical annular gaps, the heat transfer rate between concentric cylinders is the same as that calculated for coolant conduction alone if the Rayleigh number (Ra) is less than 1000, *i.e.* natural convection is suppressed when Ra is below a critical value [Fishenden and Saunders 1950]. Estimates of Ra that apply to the type of fuel elements considered in this work (*i.e.* either concentric or parallel fuel plates) are approximately two orders of magnitude below 1000. It seems reasonable then to assume that heat transfer, either between fuel plates or between fuel plates and internal or external shrouds, need take account only of heat transfer mechanisms involving thermal radiation and conduction.

(b) External surfaces

For the HIFAR fuel element investigated by Parsons [1971], the internal thimble was described as "perforated", suggesting that coolant air could readily enter it. Because of the internal diameter, the Rayleigh number estimated for the thimble is considerably greater than the critical value, hence it must be inferred that natural convective cooling occurred. For the calculations performed, data from Fishenden and Saunders [1950] and McAdams [1954] were used to deduce that for a tube having a length of 660 mm, the natural convective heat transfer coefficient can be determined from the expression

$$h = 0.27\,[T_w - T_g]^{0.25} \qquad \text{expressed in British Thermal Units,}$$

where T_w is the temperature of the wall and T_g is the temperature of the ambient air.

A further assumption has been made in the calculations - that the coolant air temperature remains constant at the ambient value throughout the transient, thereby implying that natural convection forces are strong and unimpeded in the thimble. No other heat removal mechanisms have been considered as operating on the internal surface of the FSA thimble.

When a HIFAR fuel element is in the load/unload flask, the shroud which surrounds the outside of the fuel element is contained within a stainless steel barrel (see **figure 7**). Distances between the shroud and the stainless steel barrel are, however, such that natural convection can occur. Heat removal mechanisms involving both radiation and natural convection were therefore assumed to be operating on the external surface of the shroud. Furthermore, since the two stainless steel barrels within the flask are themselves well ventilated, they were assumed to be at ambient temperature during the heating transients investigated.

3.2 ORR Fuel Elements

The nodal model used to calculate temperature responses which could be compared with experimental data can be seen in **figure 8**. This model simply represents a thick-wall cylinder which extends the full length of the fuel element, *i.e.* including the end box (see **figure 2**).

3.2.1 Material properties and heat sources

The information provided by Houghtaling *et al.* [1964] on fuel alloy properties shows that although the fuel elements used in the ORR experiments reported by Wett [1960] had different enrichments from those of the HIFAR fuel elements, the material properties were the same as those given in **section 3.1.1,** except for thermal conductivity. This property needed to be 1.654 W/cm °C in input data specifications instead of 1.341 W/cm °C.

Since data on the axial power distributions in the ORR box-type fuel element tested by Wett were not readily available, it was assumed that the axial power distribution was uniform. As discussed later, results obtained for the HIFAR fuel element indicate that such an assumption should not influence thermal responses to any significant extent. In all other respects, the specification of material properties was similar to that used for the HIFAR fuel element.

3.2.2 Thermal boundary conditions

In investigations which involved the XY cross-sectional model, it was assumed, as for the HIFAR fuel element, that heat transfer between fuel plates was only by thermal radiation and conduction through the gas.

Heat removal from the external surfaces of both the XY cross-sectional model and the equivalent RZ model was considered to be controlled by (i) thermal radiation to a sink at ambient temperature, and (ii) natural convection to air at ambient temperature. Because the heated lengths of the HIFAR fuel elements and the ORR fuel elements were very similar, the same expression as that given in **section 3.1.2(b)** was used for calculating the natural convective heat transfer coefficient.

4. RESULTS AND DISCUSSION

4.1 Preliminary Investigations

Before developing the model of the HIFAR fuel element described in **section 2.1**, a simple RZ model was formulated which was basically one-dimensional, *i.e.* it corresponded to an axially short section of the central region of a fuel element with no axial conduction, fuel plate ends or axial variations in power factor. This simple approach indicated that the predicted time to thermal equilibrium was much shorter than that observed by Parsons [1971]. It was thus reasoned that the fuel element model needed to include geometrical features which increased thermal capacity. The full length of the fuel plates, the fuel plate support combs and some representation of the fuel element beyond the level of the support combs were therefore incorporated and various preliminary investigations conducted to determine the influence of each of these features on thermal response. These calculations provided the basis for the model design.

4.2 Derivation of Surface Thermal Emissivity

After the model concept and modes of heat transfer which cool the fuel element both internally and externally had been chosen, the remaining unknown parameter affecting the dissipation of heat was surface thermal emissivity. It was assumed that the magnitude of this was independent of (i) whether surfaces were internal or external, and (ii) the time between the removal of the fuel element from the reactor and the performance of the thermal experiments.

These assumptions, together with a fixed model configuration and known heat source, enabled steady-state temperatures to be calculated for several values of thermal emissivity and, by interpolation, a thermal emissivity value to be deduced for which calculated temperatures at the axial position of the thermocouple matched the equilibrium temperature measured in one of the experiments performed by Parsons [1971]. The results from a series of thermal tests conducted by Parsons are reproduced in **table 1**.

TABLE 1
EXPERIMENTS REPORTED BY PARSONS [1971]

Test Number	Elapsed Time from Reactor Shutdown (h)	Steady-state Temperature at Thermocouple Position (°F)
1	16.75	~915
2	42.0	~707
3	107.8	545
4	178.5	464

Since, in tests 1 and 2, the extrapolated maximum (*i.e.* fuel plate 2) thermocouple steady-state temperatures were much higher than could be tolerated without the fuel element becoming damaged, they had to be curtailed well before the equilibrium condition was reached. Tests 3 and 4 were not so limited however, so the data from test 3 were used in the procedure described above to establish a value of thermal emissivity. It was thus found that for the theoretically predicted steady-state temperature to equal that determined experimentally, an emissivity value of 0.35 was required.

To determine a thermal emissivity value in this manner depends, of course, on (i) the data from which the heat generation rate is calculated during decay heating, and (ii) the geometry of the nodal model. The first of

these factors is discussed in **appendix B** and the values of thermal power output used in various calculations are given in **table 2**. In the case of the nodal model, it was considered that the geometry would need to be

TABLE 2
POWER OUTPUTS USED IN THERMAL CALCULATIONS

(a) HIFAR Experiments [Parsons 1971]

Test Number	Decay Thermal Power Output (kW)
1	1.09
2	0.73
3	0.49
4	0.39

(b) ORR Experiments [Wett 1960]

Identifying Test Information		Decay Thermal Power Output (kW)
Fuel element	OR-164	
Decay time	19.25 h	1.48
Fuel element	OR-103	
Decay time	85 h	0.389
	131 h	0.308
	154 h	0.294
	180 h	0.281

radically changed, which would necessitate significantly altering the surface thermal emissivity required to equate calculated and experimental equilibrium temperatures. The reasons for this assumption were as follows.

As described in **section 4.1**, the model design was strongly influenced by thermal transient characteristics and had to account for observed radial temperature gradients. These radial temperature gradients were affected by the fuel plate support combs and, to a lesser extent, the extended lengths for the FSA tube and external shroud. The influence on temperature responses of eliminating these two features will be discussed later but, at this juncture, it should be noted that the derived thermal emissivity value did not have to be significantly varied if the extended lengths of the FSA tube and external shroud were halved, *i.e.* when these lengths were greater than approximately 10 cm, they were not critical to steady-state temperature values. It may be concluded therefore that, although representation of the ends of the fuel element is necessary (see **section 4.3.3**), detailed modelling is not critical.

4.3 HIFAR Fuel Element

4.3.1 Steady-state temperatures

The model specified in **section 2.1**, the boundary and material conditions specified in **section 3.1**, and a thermal emissivity of 0.35 were used to calculate steady-state temperatures for the thermal power outputs in **table 2**. The results of these calculations are shown in **table 3**, which also contains, for comparison, the extrapolated steady-state temperatures indicated by Parsons' experiments.

TABLE 3
CALCULATED AND EXPERIMENTAL STEADY-STATE TEMPERATURES FOR HIFAR FUEL ELEMENT

Thermal Power Output (kW)	Equilibrium Temperatures: Extrapolated from Experimental Results (°C)	Equilibrium Temperatures: Calculated (°C)
1.09	490	477
0.73	375	368
0.49	285	285
0.39	240	244

Table 3 shows that calculated and extrapolated experimental equilibrium temperatures are in good agreement, verifying the assumption that the thermal emissivity can be taken as being constant.

4.3.2 Transient responses

Calculated and experimentally measured temperature responses for the four output powers given in **table 2** are shown on **figures 9** to **12**. The temperature responses shown on these figures are those relevant to the axial level at which experimental temperatures were measured, *i.e.* at a plane ~12 cm from the mid-plane of the fuel element. As a consequence, thermal responses shown on **figures 9** to **12** do not indicate maximum fuel plate temperatures. Normalised radial temperature distributions for different times during the transient are also included on **figures 9** to **12**.

Comparison of calculated and measured temperature transients indicates that for the four HIFAR experiments considered, the calculated rate of temperature rise in the early part of the transient is considerably greater than that measured experimentally.

In this part of the transient, the most significant parameters influencing the rate of temperature rise are the thermal capacity of the fuel element, the heat source and the experimental procedure. The method of calculating the decay heating is unlikely to be seriously in error since it has been shown to be satisfactory in analysing other experimental data. Possible explanations are that the model may underestimate, in some way, the thermal capacity of the fuel element or that the test procedure influenced the experimental results. The first of these possibilities was investigated in some depth. It was found that an increase in the thermal mass of the extended lengths of the inner and outer sheaths of the fuel element did not significantly affect the calculated initial rate of increase in fuel plate temperatures. Physical dimensions and material properties were also scrutinised to ensure that they were not in error, but no discrepancies were found. Hence, it was concluded that the difference between the rates at which the calculated and measured temperature responses increased in the initial phase of each transient could not be attributed to incorrect estimates of thermal capacity.

However, experimental procedure does offer an explanation of the differences in caculated and measured temperature responses in the initial phase of the transient. At the commencement of the transient, the irradiated fuel elements are lifted from the fuel storage block into the load/unload flask. It is quite conceivable, therefore, that when enclosed in the flask, the fuel elements are not completely dry. If this is so, then traces of water would have two effects. First, they would reduce the rate of rise in fuel plate temperature as the water evaporated and then the steam generated would increase the conductive effect of the air/steam mixture situated between the fuel plates. This would continue until the steam was expelled from the fuel element. Quantification of this explanation is however difficult, so it has to be accepted that the calculated temperature transients shown in **figures 9** to **12** are as near to experimental data as can be achieved. Acceptance of this means that the maximum discrepancy between calculated and measured temperatures occurs in HIFAR test 1 after ~15 minutes and is of the order of 70°C. The calculated results, however, are conservative in that they predict a more rapid rise in temperature than occurred in experiments.

4.3.3 Effect of geometrical and heat generation assumptions on calculated temperature responses

Earlier (**section 2.1**) it was noted, with regard to the development of the HIFAR fuel element model, that

(i) representation of the fuel element beyond the level of the support combs seemed necessary to increase the thermal capacity of the model;

(ii) inclusion of representation of the support combs enabled radial temperature distributions to be more accurately matched, and

(iii) the non-uniformity of axial power distribution should be taken into account.

To illustrate the effect of these factors on calculated thermal responses, calculations were performed in which the following were taken into account:

(a) The axial power distribution was uniform.

(b) As for (a) but with the model fuel element reduced to the level of the fuel plate support combs.

(c) As for (b) but with no representation of the fuel plate support combs.

In each of these calculations, the thermal power output was 1.09 kW (*i.e.* that for test number 1 of **table 2**) and the thermal emissivity was constant at 0.35. **Figure 13**, which contains these results and the calculated response of the complete model, shows that calculated temperature response is very little influenced by the non-uniform axial power distribution assumed for this work. In contrast, end effects significantly affect temperature responses and, in terms of thermal power output, exclusion of end effects is equivalent to having to reduce the power output by 25 per cent.

4.4 ORR Fuel Elements

4.4.1 Transient temperature responses

The equivalent cylindrical model described in **section 2.2**, the decay powers given in **table 2** and a thermal emissivity value 0.35 have been used to calculate temperature responses for comparison with experimental data obtained for ORR fuel elements OR-164 and OR-103 [Wett 1960]. In performing such calculations (apart from developing an equivalent cylindrical model to reproduce the cross-sectional area of the fuel, the total fuel element length and the external area of the fuel element), no attempt was made to match either measured steady-state or transient temperatures to calculated values. That is, no changes to thermal emissivity or coefficients of heat transfer equations were made because such changes would negate the hypothesis that temperature response can be accurately calculated, irrespective of any changes in fuel element configuration, once the theoretical principles, physical constants, and material properties of the geometrical model, and the heat removal mechanisms and heat generation rates have been established.

The calculated and experimental temperature responses given in **figures 14 and 15** show that agreement between calculated and experimental responses is good. Unlike the comparisons made for the HIFAR fuel element, there are no significant inexplicable differences between the calculated and measured temperature responses in the early part of the transient. With the ORR fuel elements, the only main difference is in the calculated and extrapolated experimental steady-state temperatures. Variations between calculated and measured transient temperatures are not, however, large, the maximum difference being less than 15°C for the periods shown on **figures 14 and 15**.

4.4.2 Axial temperature distribution

For fuel element OR-164, Wett [1960] described axial temperature profiles measured some time after the transient temperature experiments; however, he did not specify the period which had elapsed between removal of the element from the cooling pond and these measurements. This causes some difficulty when comparing calculated and measured temperatures. Nevertheless, on **figure 16** calculated temperature distributions for periods ranging from 45 min after removal of the fuel element from the cooling pond to the equilibrium condition are compared with experimental data. **Figure 16** shows that the measured axial profile is not symmetrical as was assumed in the theoretical approach. Notwithstanding this difference, **figure 16** shows that there is a strong similarity between calculated and measured axial temperature profiles. Furthermore, for the upper half of the fuel element, the maximum difference between calculated and measured temperatures ranges from 20 to 30°C, again indicating its close agreement between calculated and experimental values of temperature.

5. CONCLUSIONS

To provide a calculational basis for predicting the thermal responses of HIFAR fuel elements subjected to LOCAs, relatively simple theoretical models have been developed which can be used to analyse and reproduce experimental thermal responses obtained for irradiated fuel elements from DIDO class reactors subjected to loss of forced convective cooling. The theoretical principles relating to heat removal mechanisms, geometry, decay heat generation and physical properties for these analytical models have been formulated such that the

thermal response of any geometrical configuration can be calculated without the need for arbitrary assumptions relating to heat transfer mechanisms or thermal properties.

Comparison of calculated and experimental thermal responses for a HIFAR Mark IV/V fuel element have shown the following:

(i) The end effects of the fuel element need to be incorporated in the model since they account for approximately 25 per cent of the power dissipated; however, detailed modelling of the fuel element ends was not found to be important.

(ii) Agreement between calculated and extrapolated steady-state temperatures is excellent when the surface thermal emissivity is assumed to be 0.35.

(iii) Calculated rates of temperature rise in the initial phase of a transient are greater than those observed in experiments - this discrepancy may be due to the experimental procedure adopted.

(iv) Notwithstanding the difference between the calculated and measured rates of temperature rise in the initial phase of a transient, the maximum discrepancy between calculated and measured temperatures is ~70°C, with the calculated values being the greater.

(v) Axial power distribution did not significantly affect thermal responses.

The information gained from examining the thermal responses of a HIFAR fuel element was used to construct a theoretical model of the ORR fuel element and thermal responses were calculated to enable comparison with experimental data obtained by Wett [1960]. This comparison demonstrated two aspects:

(i) Calculated and experimental responses are in excellent agreement, the maximum difference between calculated and measured temperatures being less than 15°C.

(ii) Axial temperature distributions measured near equilibrium conditions were also in close agreement with calculated values. The calculated temperatures were approximately 20 to 30°C greater than measured values.

In summary, a relatively simple method for modelling and calculating the thermal response of DIDO type reactor fuel elements has been evolved which gives reasonably accurate predictions.

6. REFERENCES

Clancy, B.E., Connolly, J.W. [1985] - An assessment of possible events following a loss of coolant accident in HIFAR. AAEC unpublished report.

Collier, W.D. [1969] - HEATRAN - A finite element code for heat transfer problems. UKAEA TRG 1807(R).

Duerden, P. [1972] - HIFAR physics data. AAEC unpublished report.

Eckert, E.R.G., Drake, R.M. [1959] - Heat and Mass Transfer. McGraw-Hill, New York, 2nd edition.

Fishenden, M., Saunders, O.A. [1950] - An Introduction to Heat Transfer. Oxford University Press, London.

Green, W.J. [1973] - A theoretical study of the transient heat transfer performance of a HIFAR Mark IV/V fuel element when situated in stagnant air. AAEC unpublished report.

Green, W.J. [1974] - An extension of the theoretical study of the transient and steady-state heat transfer performance of a HIFAR Mark IV/V fuel element when situated in stagnant air. AAEC unpublished report.

Houghtaling, J.E., Sola, A., Spano, A.H. [1964] - Transient temperature distributions in the SPERT 1 D12/25 fuel plates. IDO 16884.

Lyman, T., ed. [1954] - Metals Handbook. American Society of Metals, Cleveland, Ohio.

McAdams, W.H [1954] - Heat Transmission. McGraw-Hill, London.

Nicholson, K.P. [1978] - Fission product decay heating in DIDO/PLUTO fuel elements. AERE-M 2959.

Parsons, N.A. [1971] - The temperature of uncooled Mk 4 fuel elements during unload from HIFAR. AAEC unpublished report.

Weast, R.C., ed. [1971] - Handbook of Chemical and Physical Constants. Chemical Rubber Company, Cleveland, Ohio, p. 51.

Wett, J.F. [1960] - Surface temperatures of irradiated ORR fuel elements cooled in stagnant air. ORNL 2892.

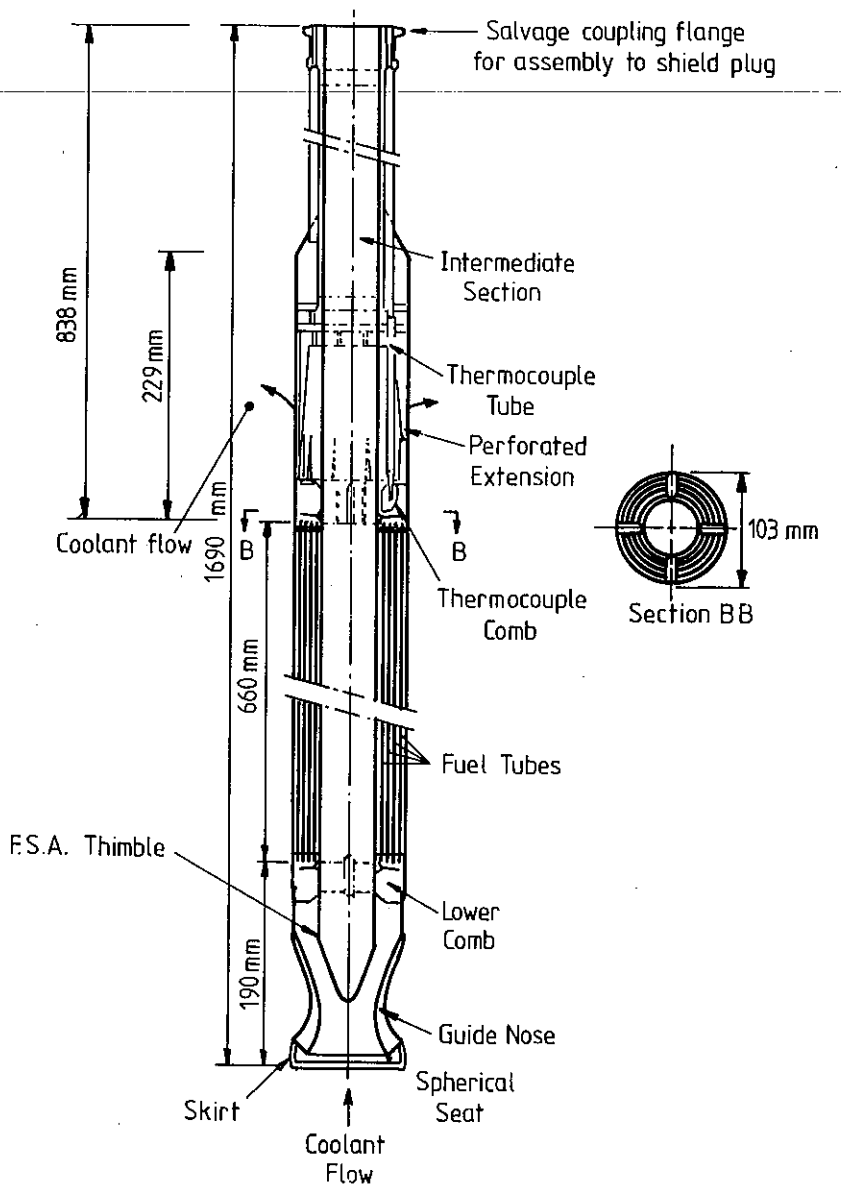

Figure 1 HIFAR Fuel Element Mark IV/5A

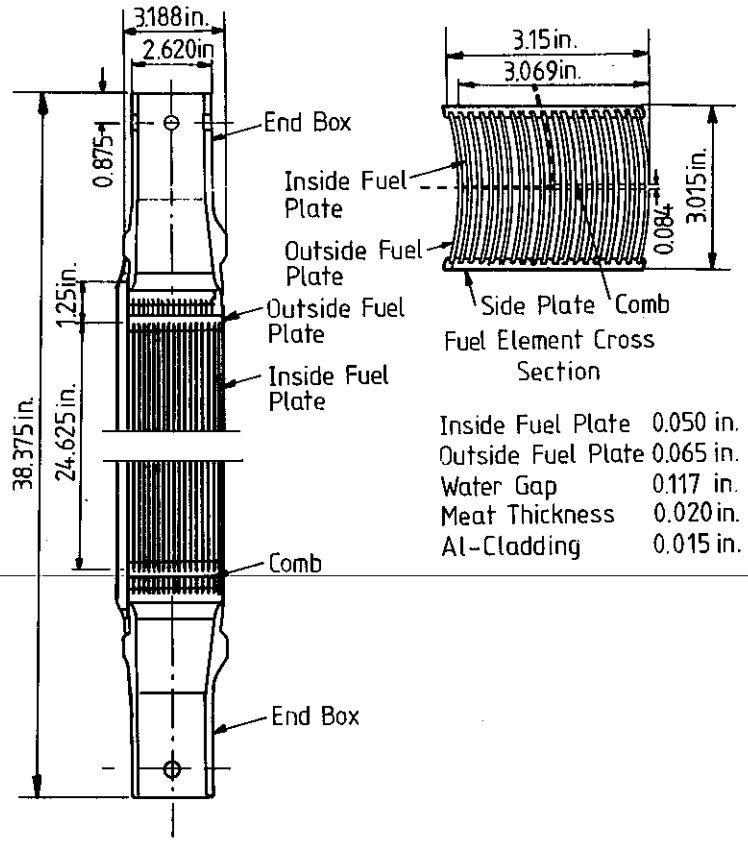

Figure 2 ORR Fuel Element

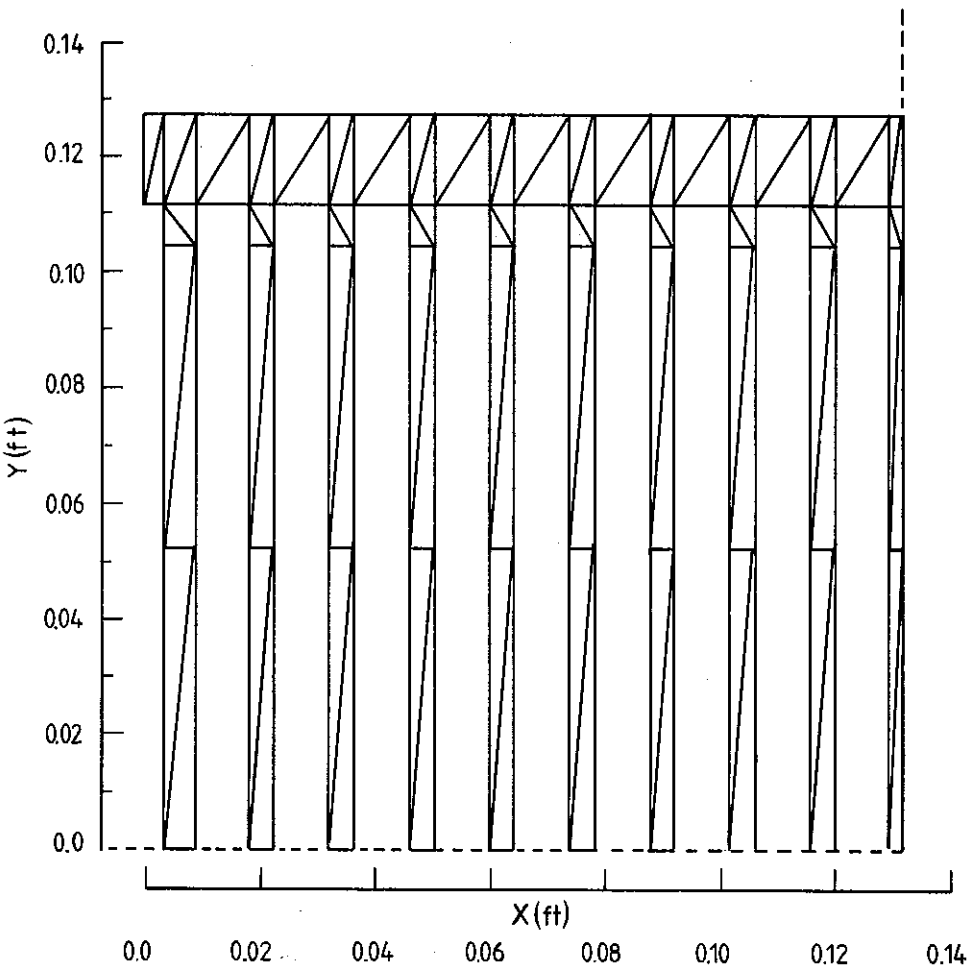

Figure 3 'XY' Model of Oak Ridge Fuel Element

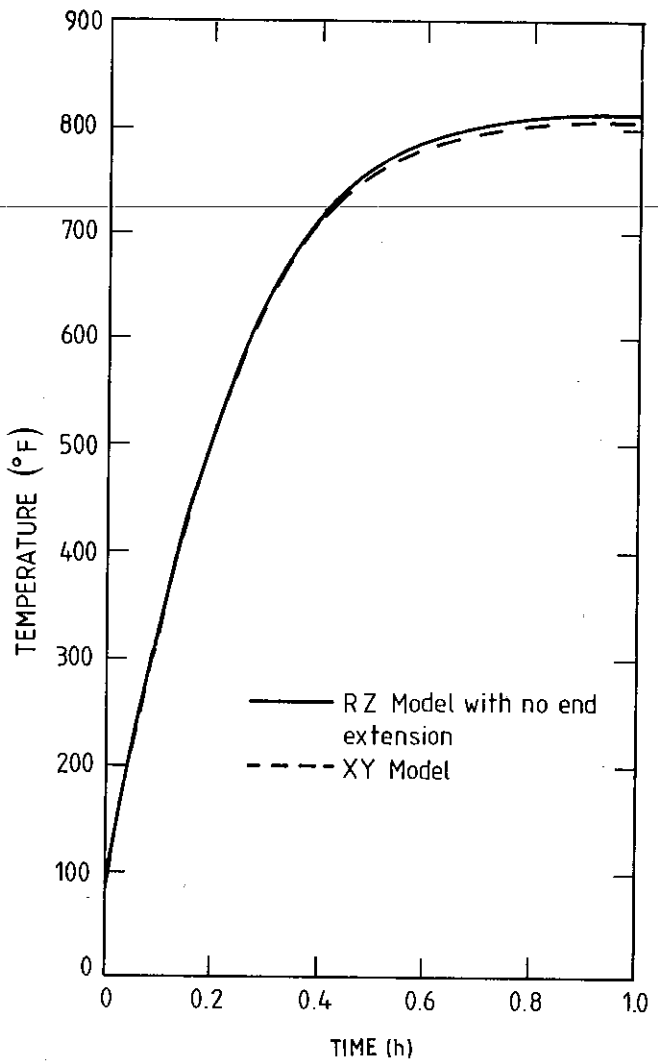

Figure 4 Comparison of RZ and XY Models of ORR Fuel Element

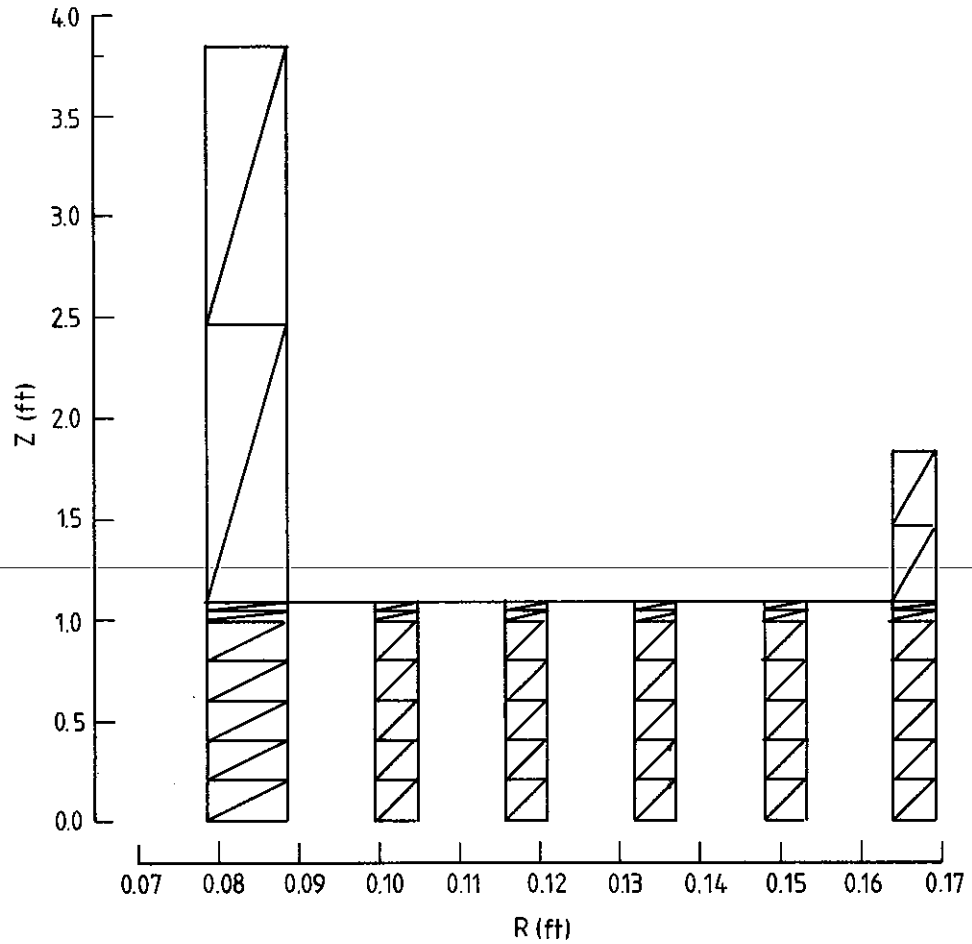

Figure 5 **RZ Model of HIFAR Fuel Element**

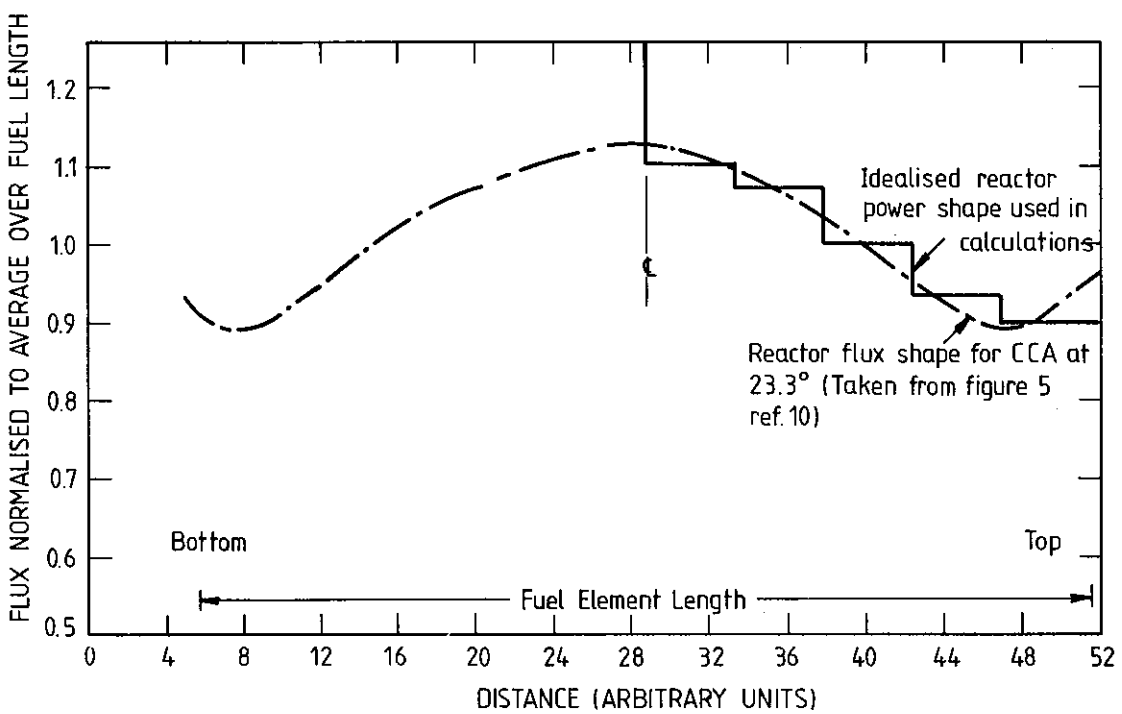

Figure 6 **Typical HIFAR Axial Flux Distribution**

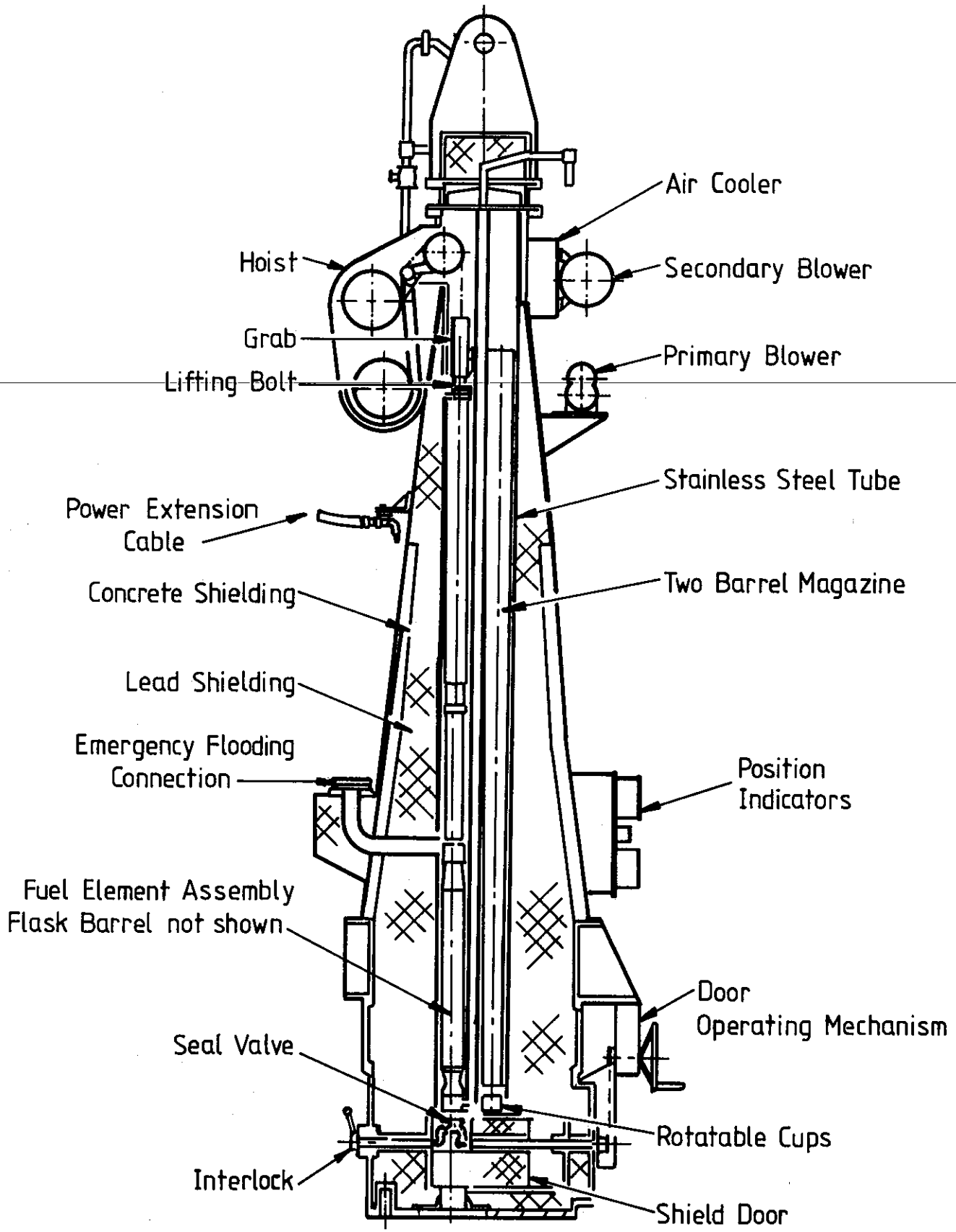

Figure 7 HIFAR Fuel Element Load/Unload Flask

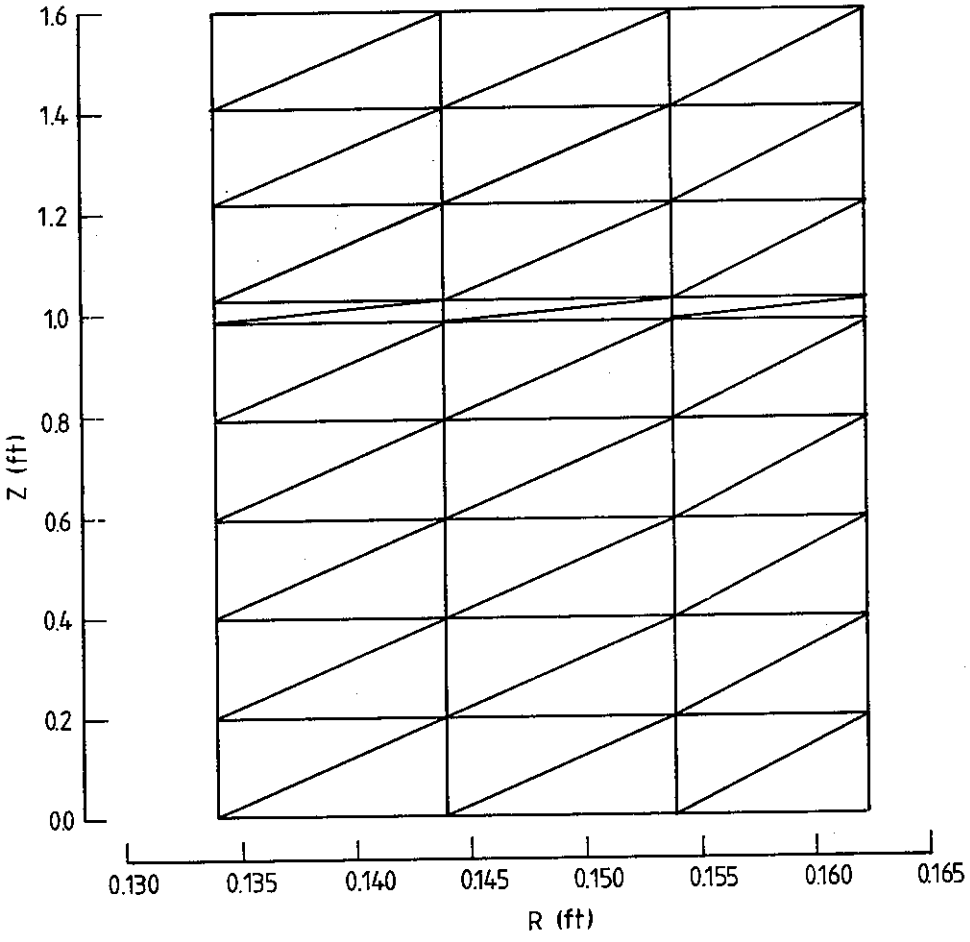

Figure 8 Equivalent RZ Model of ORR Fuel Element

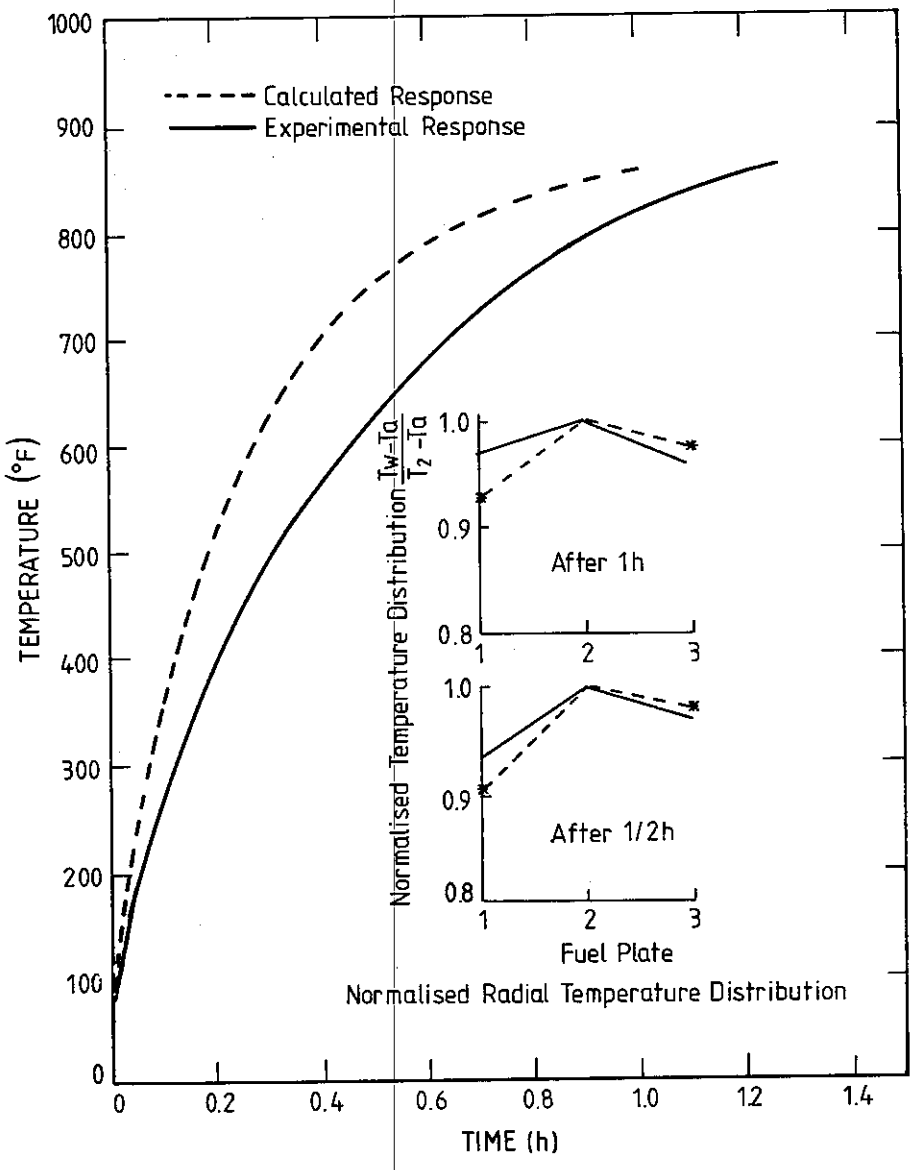

Figure 9 Thermal Response for HIFAR Test 1 of Parsons [1971]

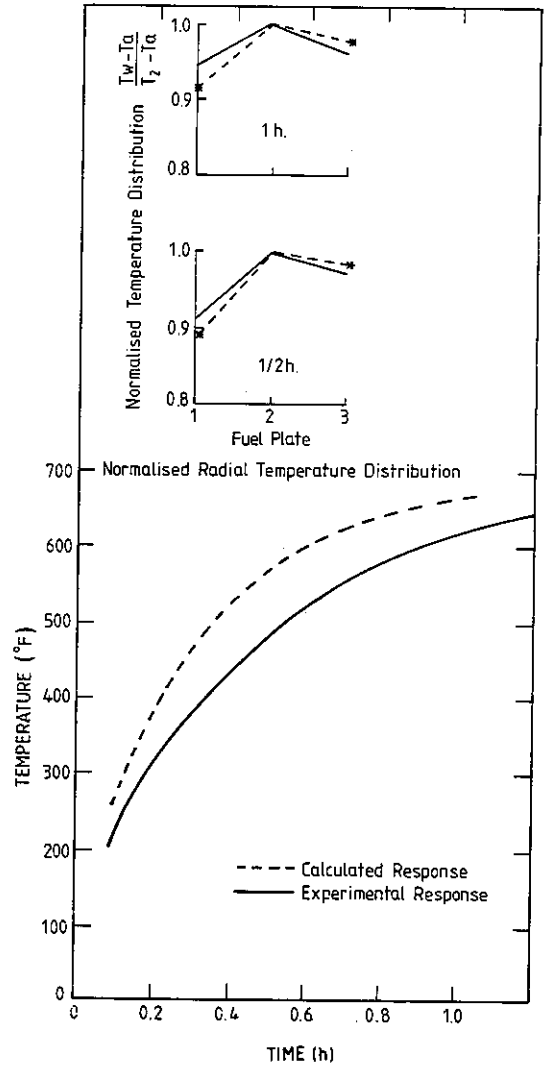

Figure 10 Thermal Response for HIFAR Fuel Element Test 2 of Parsons [1971]

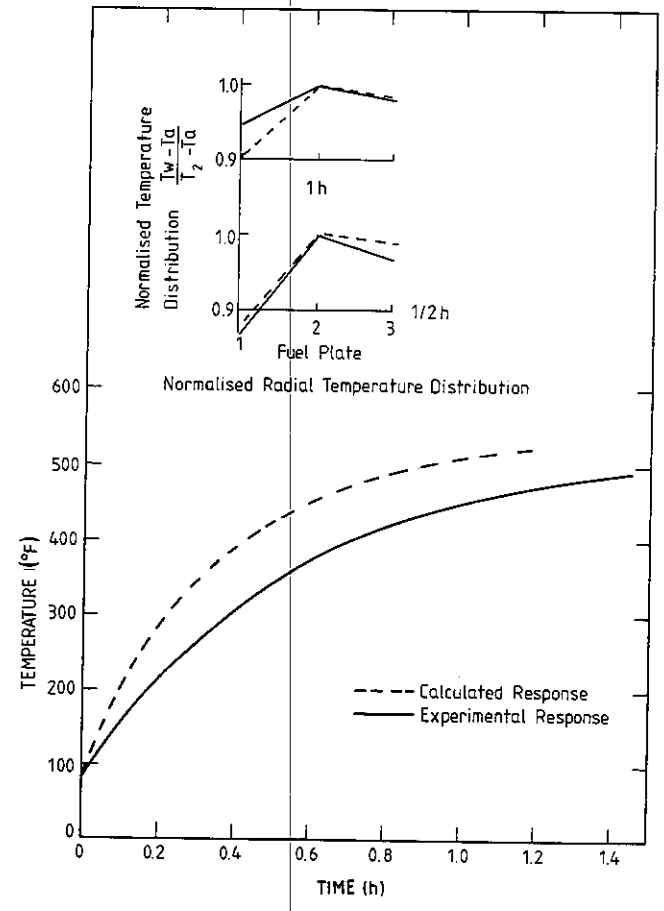

Figure 11 Thermal Response for HIFAR Fuel Element Test 3 of Parsons [1971]

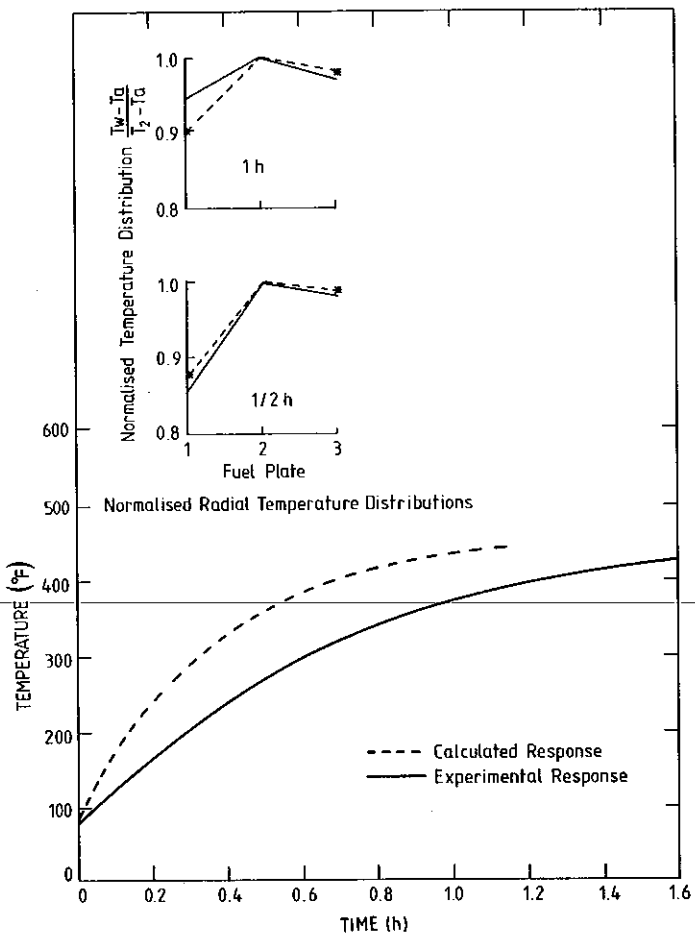

Figure 12 **Thermal Response of HIFAR Fuel Element Test 4 of Parsons [1971]**

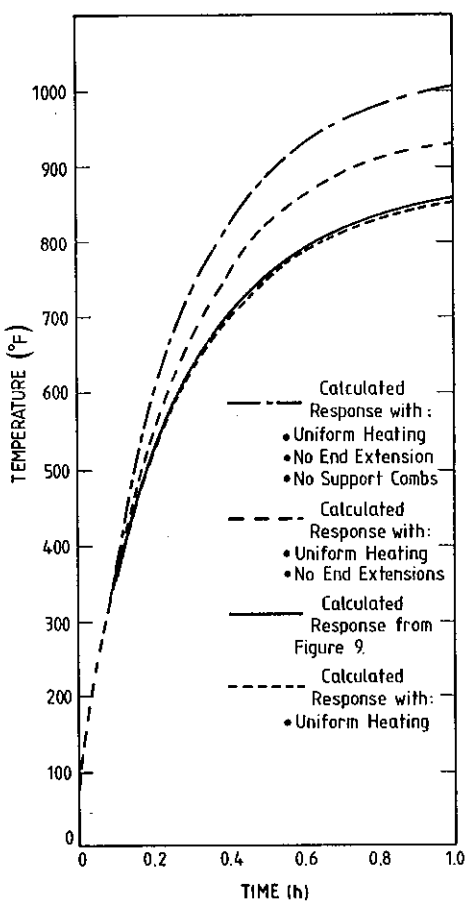

Figure 13 **Influence of Geometrical and Thermal Assumptions on Calculated Temperature Response**

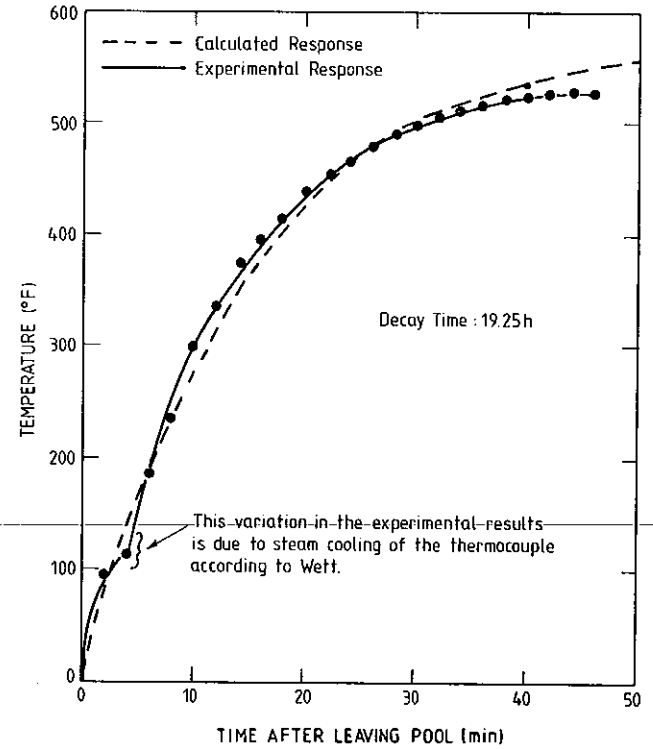

Figure 14 Calculated and Measured Temperature Transients of ORR Fuel Element Designated OR-164

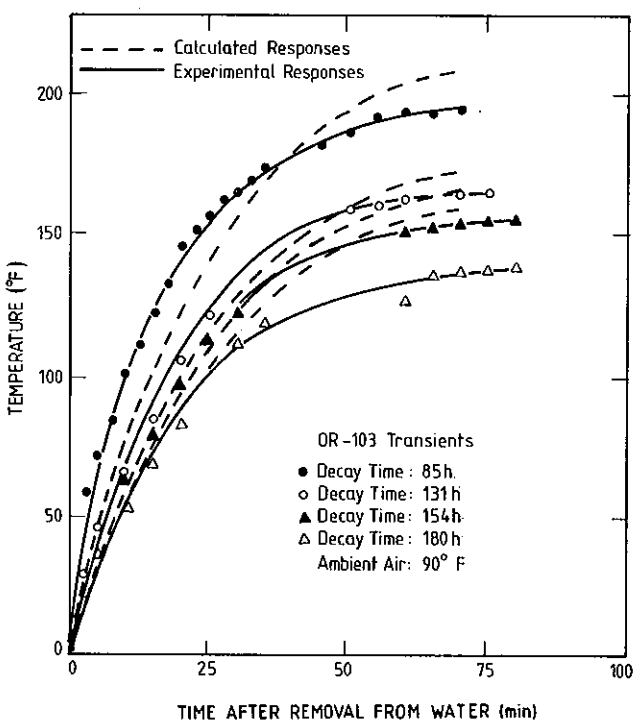

Figure 15 Calculated and Measured Temperature Transients of ORR Fuel Element Designated OR-103

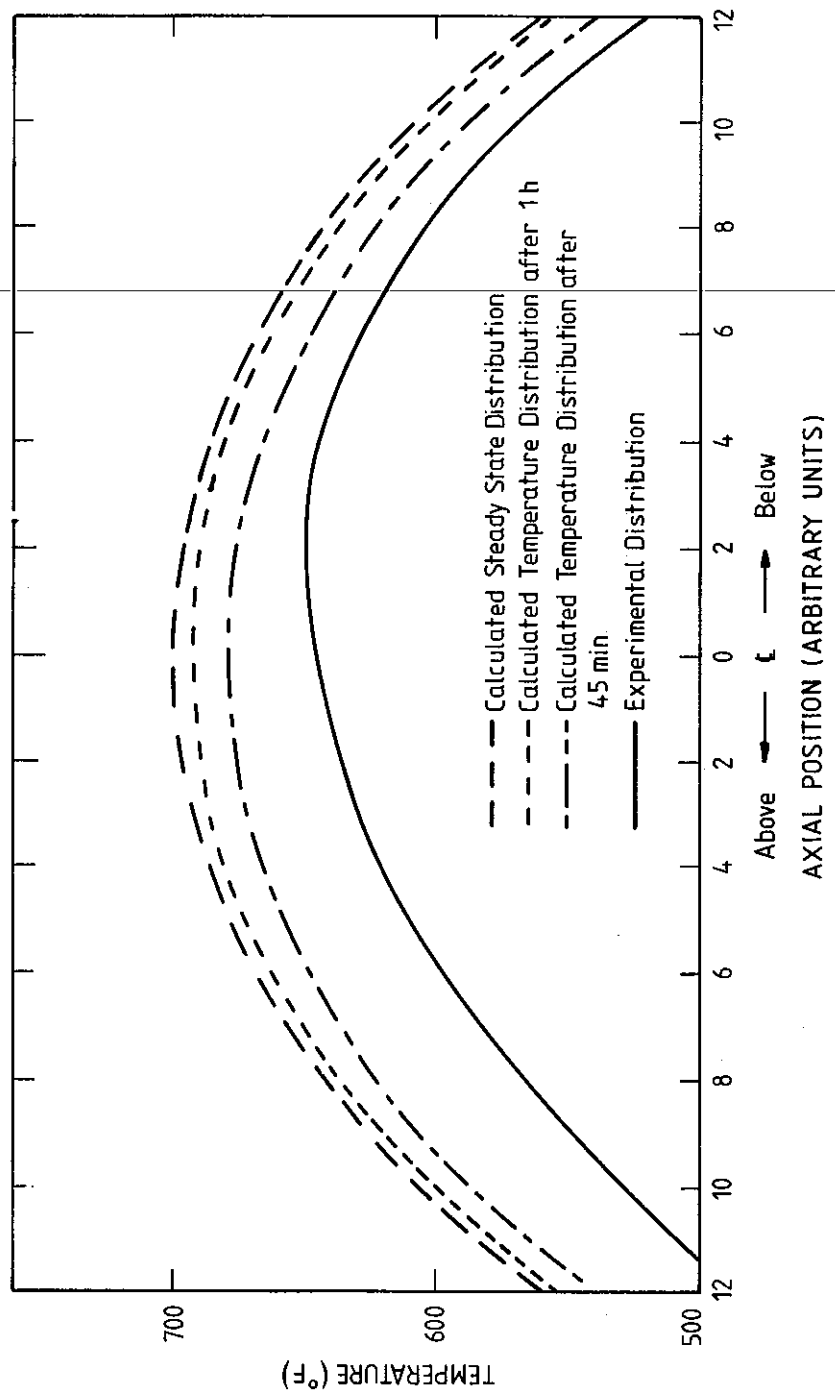

Figure 16 Steady State Axial Temperature Distribution for ORR Fuel Element OR-164: After a Decay Time of 19.25 h

APPENDIX A
LISTING OF COMPUTER INPUT CORRESPONDING TO HIFAR FUEL ELEMENT EXPERIMENTAL CONDITIONS REPORTED BY PARSONS [1971]

```
* Full length model HIFAR fuel element

GEOM RZ
NODES
1  0.0786984 0.0 ( 0.009843  0.0)
/ 0.0  0.19784  TO 6
7  0.0786984  0.99161 (  0.009843 0.0)
/ 0.0 0.05 TO 8
/ 0.0 0.04 TO 9
/ 0.0 0.00109 TO 10
/ 0.0 1.375 TO 12
13  0.09972 0.0
(0.004998 0)
/ 0.0  0.19784   TO 18
19  0.09972 0.99161
(0.004998 0)
/ 0.0 0.05 TO 20
/ 0.0 0.04 TO 21
/ 0.0 0.00109 TO 22
23  0.115802 0.0
(0.004998 0)
/ 0.0 0.19784 TO 28
29  0.115802 0.99161
(0.004998 0)
/ 0.0 0.05 TO 30
/ 0.0 0.04 TO 31
/ 0.0 0.00109 TO 32
33  0.131884 0.0
(0.004998 0)
/ 0.0 0.19784 TO 38
39  0.131884 0.99161
(0.004998 0)
/ 0.0 0.05 TO 40
/ 0.0 0.04 TO 41
/ 0.0 0.00109 TO 42
43  0.147966 0.0
(0.004998 0)
/ 0.0 0.19784 TO 48
49  0.147966 0.99161
(0.004998 0)
/ 0.0 0.05 TO 50
/ 0.0 0.04 TO 51
/ 0.0 0.00109 TO 52
53  0.164048 0.0 (   0.005166 0.0)
/ 0.0 0.19784 TO 58
59  0.164048 0.99161 (   0.005166 0.0)
/ 0.0 0.05 TO 60
/ 0.0 0.04 TO 61
/ 0.0 0.00109 TO 62
/ 0.0 0.375 TO 64
CONNECTIONS
1(1-2)(1AB2)1-2--6
7(1-2)(1AB2)7-8--12
13(1-2)(1AB2)13-14--18
19(1-2)(1AB2)19-20--22
23(1-2)(1AB2)23-24--28
29(1-2)(1AB2)29-30--32
```

```
33(1-2)(1AB2)33-34--38
39(1-2)(1AB2)39-40--42
43(1-2)(1AB2)43-44--48
49(1-2)(1AB2)49-50--52
53(1-2-3)(1AB3)53-54--58
59(1-2-3)(1AB3)59-60--64
6,1-7,1-6,2-7,2
18,1-19,1-18,2-19,2
28,1-29,1-28,2-29,2
38,1-39,1-38,2-39,2
48,1-49,1-48,2-49,2
58,1-59,1-58,2-59,2
10,2-22,1-9,2-21,1
22,2-32,1-21,2-31,1
32,2-42,1-31,2-41,1
42,2-52,1-41,2-51,1
52,2-62,1-51,2-61,1
FAHREN
MAP
INREC    0.07    0    0    10    10    1
INREC    0.09972    0    0   .004998   0.19784   2 S 1
INREC    0.115802     0    0   .004998   0.19784   2 S 1
INREC    0.131884       0    0   .004998   0.19784   2 S 1
INREC    0.147966     0    0   .004998   0.19784   2 S 1
INREC    0.09972     .19784    0   .004998   0.19784   2 S 2
INREC    0.115802      .19784    0   .004998   0.19784   2 S 2
INREC    0.131884        .19784    0   .004998   0.19784   2 S 2
INREC    0.147966      .19784    0   .004998   0.19784   2 S 2
INREC    0.09972     .39568    0   .004998   0.19784   2 S 3
INREC    0.115802      .39568    0   .004998   0.19784   2 S 3
INREC    0.131884        .39568    0   .004998   0.19784   2 S 3
INREC    0.147966      .39568    0   .004998   0.19784   2 S 3
INREC    0.09972     .59352    0   .004998   0.19784   2 S 4
INREC    0.115802      .59352    0   .004998   0.19784   2 S 4
INREC    0.131884        .59352    0   .004998   0.19784   2 S 4
INREC    0.147966      .59352    0   .004998   0.19784   2 S 4
INREC    0.09972     .79136    0   .004998   0.19784   2 S 5
INREC    0.115802      .79136    0   .004998   0.19784   2 S 5
INREC    0.131884        .79136    0   .004998   0.19784   2 S 5
INREC    0.147966      .79136    0   .004998    0.19784    2 S 5

MATERIALS
1    169    118    0.214
2   177.7   96   .208
SOURCES
1   0   130287
2   0   126733
3   0   118443
4   0   110152
5   0   106599
INIT TEMP DIST
INREC   0.07    0    0    10    10    80
```

```
TIME
0.0 0.02 0.04 0.06 0.08 0.1 0.12 0.14 0.16 0.18 0.2 0.22 0.24 0.26 0.2
0.3 0.32 0.34 0.36 0.38 0.4 0.42 0.44 0.46 0.48 0.5 0.52 0.54 0.56 0.5
0.6 0.62 0.64 0.66 0.68 0.7 0.71 0.72 0.73 0.74 0.75 0.76 0.77 0.78 0.
0.8 0.81 0.82 0.83 0.84 0.85 0.86 0.87 0.88 0.89 0.9 0.91 0.92 0.93 0.
0.95 0.96 0.97 0.98 0.99 1.
BOUNDS
1,1-1,2          1
13,1-13,2          1
23,1-23,2          1
33,1-33,2          1
43,1-43,2          1
53,1-53,2           1
10,2-22,1--62,1           1
9,2-21,1                  1
21,2-31,1                 1
31,2-41,1                 1
41,2-51,1                 1
51,2-61,1                 1
64,1-64,2           1
1,2-2,2--9,2              2
13,1-14,1--21,1           3
13,2-14,2--21,2           4
23,1-24,1--31,1           5
23,2-24,2--31,2           6
33,1-34,1--41,1           7
33,2-34,2--41,2           8
43,1-44,1--51,1           9
43,2-44,2--51,2          10
53,1-54,1--61,1          11
53,2-54,2--62,2          12
53,2-54,2--62,2    13
10,2-11,2-12,2           14
62,1-63,1-64,1           15
62,2-63,2-64,2           16
12,1-12,2          17
1,1-2,1--12,1            18
BC
1   1   0   0
2  GAP  3   .00443 .3670E-09 1. .0022009 .0022009  0  0  0  0
4  GAP  5   .00443 .3670E-09 1. .0022009 .0022009  0  0  0  0
6  GAP  7   .00443 .3670E-09 1. .0022009 .0022009  0  0  0  0
8  GAP  9   .00443 .3670E-09 1. .0022009 .0022009  0  0  0  0
10 GAP  11  .00443 .3670E-09 1. .0022009 .0022009  0  0  0  0
12  R  80  .6055E-09
13  C  80  .25  0  .27
14   1   0   0
15   1   0   0
16   1   0   0
17   1   0   0
18  C  80  .25  0  .27
ROUT PRINT
SOLVE
```

APPENDIX B
CALCULATION OF FISSION PRODUCT DECAY HEATING

Various direct measurements of decay heat have resulted in different data sets for expressing fission product decay power as a function of time from the end of irradiation. Often, then, when specifying the decay heating output of an irradiated fuel element during a thermal experiment, authors such as Parsons and Wett use different decay power data sets. After consultation with Connolly [1985, AAEC private communication] it was decided that since the American Nuclear Society had produced a best fit of decay power data sets (referred to as ANS 5.1), this consistent data set would be used to reassess decay powers at the conditions for the irradiated fuel elements tested by Parsons [1971] and Wett [1960], and in any subsequent predictive calculations.

B. McGregor (quoted in Clancy and Connolly [1975]) stated that an appropriate value for the fraction of decay power absorbed by a fuel element and converted into heat is 0.62. Nicholson [1978], however, suggested that this fraction in a single Mk 5/7 fuel element subjected to irradiation in the core for one, two or three reactor cycles at 25 MW in an average-rated position depends on the time that the fuel element has been removed from the core. Typical figures quoted by Nicholson are 0.52 and 0.45. The present analysis assumes that, for the fuel elements used by Parsons and Wett, an appropriate value is 0.51.

An example of the manner in which heat output powers were calculated is as follows. Consider a HIFAR fuel element which has been removed from the reactor for 16.75 h after having been irradiated for two reactor cycles - the first lasting ~23 days with a calculated power output of 636 kW, the second lasting ~25 days with a calculated power output of 565 kW.

Precise duration of first irradiation cycle (t_0^1)

$$= 23 \text{ days } 7 \text{ h} = 2.01 \times 10^6 \text{ s}$$

Time from end of first irradiation cycle till time of test (t_s^1)

$$= 55 \text{ days } 19 \text{ h} + 16.75 \text{ h} = 4.88 \times 10^6 \text{ s}$$

The fission product decay power from the first cycle is given by [J. Connolly, private communication]

$$\frac{P^1}{P_0^1}(t_0^1, t_s^1) = \frac{P^1}{P_0^1}(\infty, t_s^1) - \frac{P^1}{P_0^1}(\infty, t_0^1 + t_s^1)$$

where P^1 is the fission product decay power and P_0^1 is the operating power.

From the standard decay heat curve given in ANS 5.1

$$\frac{P^1}{P_0^1}(\infty, t_s^1) = 0.00155$$

$$\frac{P^1}{P_0^1}(\infty, t_0^1 + t_s^1) = 0.00135$$

Since $P_0^1 = 636$ kW

$$P^1(t_0^1, t_s^1) = 0.127 \text{ kW}.$$

Now, considering the second irradiation cycle,

$$T_s^2 = 16.75 \text{ h} = 6.03 \times 10^4 \text{ s}, \text{ and}$$

$$t_0^2 = 25 \text{ days } 9 \text{ h} = 2.19 \times 10^6 \text{ s}.$$

From ANS 5.1

$$\frac{P^2}{P_0^2}(\infty, t_s^2) = 0.00560, \text{ and}$$

$$\frac{P^2}{P_0^2}(\infty, t_s^2 + t_0^2) = 0.00205$$

$$\text{Since } P_0^2 = 565 \text{ kW}$$

$$P^2 = 2.00 \text{ kW}$$

Thus the total decay power = P^1+P^2 = 2.13 kW which, when multiplied by a factor of 0.51, leads to a thermal power output of 1.09 kW.